Internal Conversion versus Intersystem Crossing: What Drives the Gas Phase Dynamics of Cyclic α,β-Enones?

Oliver Schalk,[1,2,3] Michael S. Schuurman,[3] Guorong Wu,[4,5] Peter Lang,[2] Melanie Mucke,[6] Raimund Feifel,[6] and Albert Stolow[3,*]

[1] *Department of Physics, AlbaNova University Center, Stockholm University, Roslagstullsbacken 21, 109 61 Stockholm, Sweden*

[2] *Lehrstuhl für BioMolekulare Optik, Ludwig-Maximilians-Universität, Oettingenstraße 67, 80538 München, Germany*

[3] *National Research Council of Canada, 100 Sussex Drive, Ottawa, K1A 0R6, Canada*

[4] *State Key Laboratory of Molecular Reaction Dynamics, Dalian Institute of Chemical Physics, Chinese Academy of Sciences, Dalian, Liaoning 116023, P. R. China*

[5] *Synergetic Innovation Center of Quantum Information & Quantum Physics, University of Science and Technology of China, Hefei, Anhui 230026, P. R. China*

[6] *Department of Physics and Astronomy, Uppsala University, Box 516, 751 20 Uppsala, Sweden*

Abstract

We investigate the competition between intersystem crossing (ISC) and internal conversion (IC) as non-radiative relaxation pathways in cyclic α,β-unsaturated enones following excitation to their lowest lying $^1\pi\pi^*$ state, by means of time-resolved photoelectron spectroscopy and *ab initio* computation. Upon excitation, the $^1\pi\pi^*$ state of 2-cyclopentenone

decays to the lowest-lying $^1n\pi^*$ state within 120 ± 20 femtoseconds. Within 1.2 ± 0.2 picoseconds, the molecule subsequently decays to the triplet manifold and the singlet ground state, with quantum yields of 0.35 and 0.65, respectively. The corresponding dynamics in modified derivatives, obtained by selective methylation, show a decrease in both IC and ISC rates, with the quantum yields of ISC varying between 0.35 and 0.08. The rapid rates of ISC are explained by a large spin orbit coupling of 45-60 cm^{-1} over an extended region of near degeneracy between the singlet and triplet state. Furthermore, the rate of IC is depressed by the existence of a well-defined minimum on the $^1n\pi^*$ potential energy surface. The non-adiabatic pathways evinced by the present results highlight the fact that these molecular systems conceptually represent "intermediate cases" between ultrafast dynamics mediated by vibrational motions at conical intersections versus those by statistical decay mechanisms.

I. INTRODUCTION

The class of molecules denoted α,β-enones are a basic building block of organic synthesis and are known to manifest a varied photochemistry [1-4]. Their excited state processes, the subject of this work, involve an initial excitation to the lowest lying $^1\pi\pi^*$ (S_2) state whose absorption spectrum peaks in the wavelength range between 250 and 200 nm. Following preparation of this bright state, the dynamics exhibit rapid internal conversion to a lower lying $^1n\pi^*$ (S_1) state. The electronic structure of this state is characterized by an excitation from the non-bonding lone pair orbital on the oxygen atom to a delocalized anti-bonding π^* orbital, thereby reducing the electronic density at the oxygen, as well as its reactivity. From the $^1n\pi^*$ state, there exist two major non-radiative relaxation channels: either internal conversion (IC) to the electronic ground state or intersystem crossing (ISC) to the triplet manifold. Regarding the latter channel, two triplet states are energetically

accessible: a $^3\pi\pi^*$- and $^3n\pi^*$ state. The specific energetic ordering of these triplet states relative to the $^1n\pi^*$ state in the vicinity of the global minimum of the S_1 surface varies for the different enones, but all three states are generally close in energy [5, 6]. Non-radiative transitions from the $^1n\pi^*$ state can occur to either the $^3\pi\pi^*$- or the $^3n\pi^*$ state [7], the former being preferred according to El-Sayed's rules [8]. The subsequent ISC back to the ground state was previously studied from both triplet states [9, 10].

Most photochemical reactions of α,β-enones are known to originate from the triplet state [4]. In the gas phase, these are mostly Norrish type I reactions [4], i.e. α-cleavage reactions at the carbonyl group, or Norrish type II, if a γ H-atom is present, leading to creation of a dienole or a cyclobutane, which may then undergo several consecutive reactions [1]. Reactions in liquid phase were observed to be more varied. An overview of the many possible reactions can be found in [3].

In this study, we are interested in the fundamental question as to when and why intersystem crossing can successfully compete with internal conversion on the femto- to picosecond timescales. The molecule acrolein serves as a natural starting point to address this question. It is the simplest α,β-enone and, as such, has been studied in some detail [11-16] (see Figure 1 for the molecular structure). In the liquid phase, two major product channels are observed upon photoexcitation to the $^1\pi\pi^*$ state: [1,3] H-migration with a product yield of 0.78 and α-hydrogen loss with a product yield of 0.12 [11]. Use of a triplet quencher revealed that the first process is correlated with the triplet state whereas the second process takes place exclusively on the singlet manifold. On the basis of these results, it was concluded that ISC occurs much more readily than IC. As an explanation, it was argued that the minimum energy geometry on the $^1n\pi*$ state interacts with nearby $^3\pi\pi^*$ and $^3n\pi^*$ triplet states in acetonitrile

solution (B3LYP/cc-pVDZ with the PCM solvent model) [10]. However, absolute branching ratios are not known and it is likely that molecules reaching the ground state directly via a S_0-$^1n\pi^*$ intersection are readily cooled in solution and therefore do not show fragmentation.

An even larger uncertainty exists for branching ratios in gas phase experiments. C-H bond fission in the aldehyde functional group of acrolein was presumed to happen on the triplet surfaces, evincing gas phase ISC [12]. Lee *et al*. studied time resolved photoelectron spectra of acrolein and its monomethylated derivatives (at the α-, β-, and γ-positions, respectively): methyl vinyl ketone (MVK), methacrolein and crotonaldehyde [13]. Upon excitation of acrolein to the $^1\pi\pi^*$ state at 209 nm, an initial S_2-S_1 internal conversion was observed within approximately 100 fs and the signal associated with the $^1n\pi^*$ state decayed within (0.9 ± 0.1) ps (see Figure 2 for an overview of the dynamics). Moreover, linewidth measurements at the $^1n\pi^*$ state minimum showed a lower bound for ISC of 1.8-2.1 ps [17] which is supported by a large calculated spin-orbit coupling of ~65 cm^{-1} [18]. These experiments indicate that, following excitation of the $^1\pi\pi^*$ state, ISC is able to compete with IC in most of the simple enones. Surprisingly, a negligible triplet yield was observed for crotonaldehyde where the $^1n\pi^*$ state exhibits a decay time constant of (0.5 ± 0.07) ps [13] and HCO (α-cleavage) product formation – an indicator of ISC – could not be detected [15] (although there remains the possibility that the presence of a γ-hydrogen opens up a more efficient triplet channel competing with HCO loss). It was concluded that IC for crotonaldehyde is fast compared to that of acrolein mainly because of the more adiabatic behaviour associated with the slower torsional dynamics that result from methyl substitution [13].

Most time resolved experiments [19-21] and *ab initio* calculations [10, 22] on 2-

cyclopentanone (CPO) and related cyclic α,β-enones have dealt exclusively with triplet state dynamics, which are not the focus of this investigation. Most recently, it was shown in femtosecond time-resolved transient absorption studies that excitation of the $^1\pi\pi^*$ state of 3-methyl-2-cyclopentenone (3MeCPO) in acetonitrile and 2,3,4,5-tetramethyl-2-cyclopentenone (TMCPO) in acetonitrile and methanol led to a ground state bleach in the 230 nm region, with a time independent amplitude within the first nanosecond. This was interpreted as unit triplet quantum yield Φ_{ISC} [23, 24], and is consistent with the increased Φ_{ISC} found for acrolein upon solvation [12].

Here we investigate a series of cyclic α,β-enones: CPO, the methylated species 3MeCPO and TMCPO, as well as the open chain molecule MVK, all depicted in Figure 1. Although the electronic structures of these species are qualitatively similar, several subtle differences exist which may have significant impacts on the dynamics. Upon methylation: (i) the $^1\pi\pi*$ state is shifted to the red while the $^1n\pi*$ state is shifted to the blue (see Figure 3); (ii) the $^3n\pi^*$- and $^3\pi\pi^*$-triplet states are shifted to lower energies with respect to the $^1n\pi^*$ state at its minimum geometry (see Table 1); (iii) the closed ring structure presents a significant constraint to gradient directed (large amplitude) nuclear motions [25, 26].

The aim of the present study is to resolve the competing mechanisms which drive the primary excited state dynamics of α,β-enones and to quantify how they may be influenced by a change of dynamical parameters, e.g. increased inertia due to methylation of specific vibrational motions, and increased flexibility within certain modes by ring enlargement. Here, we combine time-resolved photoelectron spectroscopy and *ab initio* calculations to interrogate the excited state dynamics of these various substituted cyclopentenones, employing the open chain methyl vinyl ketone (MVK) as a reference, in order to clarify the reaction timescales and branching ratios between IC and ISC in these systems.

II. METHODS

A. Experimental

CPO, 3MeCPO, TMCPO, and MVK were purchased from Sigma-Aldrich with nominal purities of 98%, 97%, 95%, and 99%, respectively. For the absorption spectra and the TRPES experiments, these were used without further purification. For He(I)-photoelectron spectroscopy, the samples were degassed to remove air from the sample.

Absorption spectra were taken in a 1 cm quartz cuvette under saturated vapor pressure using a Cary 5e photospectrometer (Varian). He (I) photoelectron spectra were recorded with a magnetic bottle electron spectrometer setup akin to the one described previously in [27], but with a flight tube of 2.2 m [28, 29]. The magnetic bottle setup used for time resolved measurements is described in reference [30]. Wavelengths for pump (λ_p=216 nm) and probe (λ_e=267 nm) pulses were generated using methods analogous to those in reference [25] and the *in situ* cross correlation of the experiment was 140 fs, as measured in nitric oxide TRPES (which also served for energy calibration). The molecular beam was generated by a pulsed Even-Lavie valve with a 200 μm conical nozzle [31]. Filter paper saturated with the specific liquid sample under study was inserted into the body of the pulsed valve, providing the seed gas for the molecular beam. Expansion of the seed vapor into the vacuum system was achieved using 3 bar of helium carrier gas.

B. Theory

The energetically accessible IC relaxation pathways were investigated via optimization of the pertinent ground and excited state minimum structures, as well as low-lying minimum energy conical intersections for CPO, 3MeCPO and TMCPO. Each

computation employed an atomic natural orbital (ANO) basis set [32] of the form 3s2p1d for the C and O atoms and 2s1p for the H atoms. Those computations that involved the determination of a complete active space self-consistent field (CASSCF) reference function employed an active space denoted (5o,6e), comprised of the π, π* and lone pair σ orbital of oxygen.

The optimization of the ground state geometries were performed at the CCSD(T) level of theory determined using the CFOUR program package [33]. All excited state optimizations (i.e. energy minima and conical intersections) employed a treatment of dynamic electron correlation at the second-order multi-reference configuration interaction (SO-MRCI) level of theory for CPO and first-order (FO)-MRCI treatment for 3MeCPO and TMCPO using the COLUMBUS electronic structure package [34]. The Cartesian geometries of each optimized structure are given in Tables S1 to S20 of the Supporting Information.

At each minimum energy structure, the singlet and triplet electronic energies were computed at the Davidson-corrected SO-MRCI level of theory [35]. Table 1 summarizes the minimum energy structures, while Table 2 gives the energies at the minimum energy conical intersections. At these same geometries, the spin-orbit coupling matrix elements were computed using the ANO basis mentioned above, employing MS-CASPT2 wave-functions obtained from the MOLPRO program package [36].

III. RESULTS

A. Static Spectroscopy

Gas phase absorption spectra of CPO, 3MeCPO, and TMCPO are shown in Figure 3. As can be seen, the intense $^1\pi\pi^*$-spectra shown in the main panel exhibit a red-shift of the maximum upon increasing substitution. The opposite is true for the $^1n\pi^*$ state (see inset of

Figure 3) where increasing substitution lowers the energy of the non-bonding lone-pair orbital, yielding a small spectral blue shift (this is more clearly seen in liquid phase spectra as shown in Reference [23]).

The He(I) photoelectron spectra of CPO, 3MeCPO, and TMCPO, which serve as reference data for the interpretation of the time-resolved photoelectron spectra studied here, are shown in Figure S7 of the Supporting Information. The photoelectron spectrum of CPO is similar to those of the open chain α,β-enones acrolein and methyl vinyl ketone (MVK) [37, 38] and exhibits its first two maxima at 9.55 and 10.35 eV. According to our MRCI calculations, and in agreement with previous computations [37], the ionic ground state (D_0) is associated with ionization of the highest lying *n*-orbital, while the first excited state (D_1) is due to ionization from the π-orbital localized at the oxygen atom (see a sketch in Figure S9 in the Supporting Information). In 3MeCPO, these two bands are closer together, at 9.3 and 9.7 eV, whereas in TMCPO, only one peak at 9.3 eV can be identified.

B. *Ab initio* Electronic Structure Calculations

As shown in Table 1, the blue and red shifts of the excitation energies for the lowest lying $^1n\pi^*$ and $^1\pi\pi^*$ states are reproduced by our *ab initio* electronic structure calculations. With respect to the initial excitation, the computed vertical excitation energy of 6.17 eV for CPO agrees well with the absorption maximum at 6.11 eV. Upon methylation, the corresponding transition in 3MeCPO and TMCPO shifts to lower energy, in agreement with the maxima of the absorption spectra, although the computed transition energies of 6.11 eV and 5.84 eV are slightly higher than the observed maxima at 5.90 eV and 5.56 eV, respectively. Likewise, the computations show a clear blue-shift of the $^1n\pi^*$ state upon methylation, with the vertical excitation energies for CPO, 3MeCPO and TMCPO computed

to be 4.01, 4.05, and 4.18 eV, respectively. However, direct comparison to the experimental UV absorption spectrum is difficult as the bands are broad and of low intensity. The former observation is consistent with the sizable relaxation energies (from the Franck-Condon region) of the $^1n\pi^*$ states, shown in Table 1 to be approximately 0.4 eV for each of the CPO-derived species.

The energetic ordering of the triplet states is also given in Table 1. These show clearly that the singlet states of interest in this study are very nearly "bracketed" by pairs of triplet states over a large variety of molecular configurations. In particular, we note that the energy differences between the $^1n\pi^*$- and the T_1- and T_2 states are small over a region of configuration space which extends from the Franck-Condon (S_0 minimum) geometry to the $^1n\pi^*$- minima for CPO and both of the methyl-substituted derivatives.

Excited state seams of conical intersection were determined for a number of different crossing archetypes. Table 2 summarizes the electronic energies at those minimum energy conical intersections of relevance to this study (given the energy of the initial pump photon). As stated above, the initial non-adiabatic transition involves a conical intersection between the initially prepared $^1\pi\pi^*$ state and the lower-lying $^1n\pi^*$ state. The two primary relaxation pathways which lie below the excitation energy involve the familiar twist-pyramidalization at the C-C double bond [26, 39] in the CPO ring, as well as α-cleavage of the bond between the carbonyl carbon and an sp^3-ring carbon atom (thereby preserving the π electronic system). While the twisted-pyramidalized minimum energy conical intersection (MECI) type is slightly lower in energy than the α-cleavage intersection (by ~ 0.1, 0.3, and 0.6 eV for CPO, 3MeCPO, and TMCPO, respectively), the branching between these pathways will likely be strongly dependent on dynamical effects.

Table 2 shows that each of the S_2-S_1 intersection types has a corresponding S_1-S_0 conical intersection in both energetic and geometric proximity. Indeed, the relatively small energy gaps between S_0, S_1, and S_2 at the S_2-S_1 MECIs strongly suggest that there are seams of three state conical intersections at low-energy, although these seams were not determined in this study. In general, the S_1-S_0 MECIs lie slightly higher in energy relative to the S1-minimum (which exhibits clear $^1n\pi^*$-character). The barrier to accessing the α-cleavage MECI is relatively insensitive to the degree of methylation and is computed to be 0.37, 0.32, and 0.33 eV for CPO, 3MeCPO, and TMCPO, respectively. Alternatively, the barriers to the twisted-pyramidalized MECIs are larger and significantly influenced by methylation with energies of 1.23, 0.80, and 1.04 eV for the same three molecular species.

Lastly, the computed spin-orbit matrix elements are found to be largely geometry independent and only weakly dependent on the degree of methylation. Specifically, values of 36 and 37 cm^{-1} were determined for the spin-orbit coupling matrix elements between the $^1n\pi^*$ state and the nearest triplet states at the Franck-Condon and the $^1n\pi^*$-minimum energy geometry, respectively. These values increase to 43, 44 cm^{-1} and 48, 49 cm^{-1} for 3MeCPO and TMCPO, respectively.

C. Time Resolved Photoelectron Spectroscopy

Time resolved photoelectron spectra of CPO, 3MeCPO and TMCPO excited at 216 nm and probed at 267 nm are shown in Figure 4, whereas the corresponding spectrum of MVK is given in the Supporting Information. The total energy of one pump plus one probe photon [1+1'] is 10.38 eV, whereas probing with two photons [1+2'] delivers 15.03 eV. For CPO, the ionic ground state (D_0) is reached by [1+1'] ionization with an excess energy of

~0.8 eV which can be converted to kinetic energy of the photoelectron. This energy is in agreement with the cut-off of the intense maximum at low kinetic energies in the time resolved photoelectron spectrum (Figure 4 a) which has its origin around time zero. While ionization of the $^1\pi\pi^*$ state correlates at zeroth order to the D_1 cationic state via Koopmans' correlations, this channel exceeds the [1+1'] available energy and therefore is only energetically accessible via a multi-photon ionization of the excited state (see Figure 2). These ionization channels are in fact observed (specifically, two-photon probe ionization) at higher electron kinetic energies, as expected. Here, we see a delayed rise of the signal which can be attributed to the lower lying $^1n\pi^*$ state and is best seen in the energy slices of Figure 4c. At long delay times (> 10 ps), the spectrum retains a significant contribution which does not decay over the scan range of the measurement. The origin of this band is probably not the hot ground state since the Franck-Condon overlap with the ionic manifold is typically rather poor [40]. We suggest that this signal most likely originates from the triplet manifold.

Time constants and their Decay Associated Spectra (DAS) were determined by a Levenberg-Marquart 2D global fitting routine, as explained in detail in Reference [41]. In brief: The time- and energy-resolved photoelectron signal $S(E,\Delta t)$ can be described as a sum of *i* kinetic steps through

$$S(E,\Delta t) = \sum_i A_i(E) P_i(\Delta t) \otimes g(\Delta t) \quad (1)$$

where $A_i(E)$ is the DAS of the individual step. The DAS $A_i(E)$ has a time dependence $P_i(t)$ which is commonly expressed in terms of exponential functions; g(t) is the independently determined cross-correlation function (see experimental section). As discussed previously [26, 41, 42], this global fitting scheme may be unsatisfactory if the molecule undergoes large amplitude motions. In such cases, the spectrum typically shows a shift ('tilt') toward lower kinetic energies at longer time delays , since the vertical ionization potential typically rises

along large amplitude deformation coordinates. One phenomenological method to account for this shift within 2D global fitting is to artificially vary the 'time zero' of the fit as a parameter [26], as discussed in the Supporting Information. With such an approach, the variation in 'time zero' can be phenomenologically associated with large amplitude motion.

In the time resolved photoelectron spectrum of CPO as well as in that of MVK, no spectral shifts were observed and the time constants obtained by Equation (1) are given in Table 3. In accordance with the previous analysis, the first time constant, τ_1, can be assigned to the initially populated $S_2(\pi\pi^*)$ state whereas τ_2 is associated with the dynamics in $S_1(n\pi^*)$. For 3MeCPO and TMCPO, we see a spectral shift ('tilt') of the signal toward lower electron kinetic energies in the [1+1'] region by 20 fs (3MeCPO) and 40 fs (TMCPO) and a concomitant increase in the associated time constant. This is caused by nuclear motion toward the highly distorted conical intersection between the $^1\pi\pi^*$- and the $^1n\pi^*$ state (see Figures 2 and 5). This motion is sensitive to substitution in the 3-position as can also be inferred from the results on acrolein where a 90 degree twist of the terminal C-atom is a prerequisite for these dynamics [13]. This might not only result in slower nuclear dynamics, but also a change in the potential energy surfaces which causes the 'tilt' to become visible. This 'tilt' agrees with the work of Lee *et al.* where a similar behavior was indicated by an increase of the first time constant toward lower lying electron kinetic energies of the time-resolved photoelectron spectra of the open chained enones [13]. The time constants given in Table 3 for 3MeCPO and TMCPO include the spectral shift plus the exponential decay time at low kinetic energies (see Supporting Information).

IV. DISCUSSION

A. Determination of quantum yields

In order to discuss the influence of the triplet channel on the reaction dynamics, one must first determine approximate yields of triplet vs. singlet products from the spectroscopic results. To this end, we consider the bifurcation of the wavepacket upon reaching the conical intersection between the $^1n\pi^*$- and $^1\pi\pi^*$ states. The total decay of the excited state wavepacket via all channels occurs in about a picosecond for all of the molecules in this study, with the exception of TMCPO, where the $^1n\pi^*$ state lifetime is 2.8 ± 0.5 ps. A relative measure for the singlet-triplet branching ratio is the amplitude ratio of the so called state associated spectra (SAS) of the $^1n\pi^*$- and the triplet state which can be extracted (with the assumption of unit ionization cross sections) from the DAS, and the time constants as detailed in the Supporting Information. This ratio is shown in Figure 6 for CPO, 3MeCPO, TMCPO, and MVK. For MVK, the amplitude of the long lived component is small over the whole spectral region, in agreement with previous findings which yielded a low ISC rate for the open chained enones [13]. For TMCPO and 3MeCPO, we find this ratio increased, implying that a larger fraction of the wavepacket evolves into triplet character. The largest value of this ratio is observed for CPO. If we assume similar ionization cross-sections for all molecules, the relative triplet quantum yields Φ_{ISC} are obtained from the ratio of the energy integrated SAS for the $^1n\pi^*$- and the triple state and are 1.2 : 2.1 : 2.3 : 3.5 for MVK : TMCPO : 3MeCPO : CPO respectively. We note that these ratios may also be estimated from Figure 6 (see also Table 3). More details on this estimation procedure are presented in the Supporting Information.

Approximate triplet quantum yields can be obtained from the jet cooled fluorescence excitation spectrum of the $^1n\pi^*$ state of CPO [43]. Here, a FWHM linewidth of $\Gamma \approx 1.5$ cm$^-$

^{1}for the 0-0 transition was seen in the excitation spectrum, corresponding to a lifetime of $\tau_{ISC} = (2\pi c\Gamma)^{-1} \approx 3.5$ ps. This lifetime can be assigned to ISC since the quantum yield upon excitation to the $^1n\pi^*$ state is assumed to be unity [19]. In the following analysis, it is assumed that this rate does not change upon excitation to the $^1\pi\pi^*$ state. Employing this assumption, the quantum yield for ISC can be obtained by $\Phi_{ISC} = \tau_2 / \tau_{ISC} \approx 0.35$ and the time constant for IC is given by $\tau_{IC} = \tau_2 / (1 - \Phi_{ISC}) = 1.8$ ps. The triplet yields for the different molecules can now be estimated by the ratios derived earlier: the time constants for IC and ISC are summarized in Table 3. The following trend is observed: the rate of ISC decreases upon methylation as well as upon ring enlargement. While the rate of IC is only weakly influenced by methylation at the 3-position, it is significantly slowed upon tetra-methylation.

B. Competition between non-radiative relaxation pathways

The triplet quantum yield upon photoexcitation of α,β-unsaturated enones depends on the pump wavelength. Upon direct excitation to the origin of the $^1n\pi^*$ state, ISC is the only observed relaxation pathway [19]. This is consistent with our *ab initio* calculations which show significant potential energy barriers to accessing the relevant minimum energy conical intersections which would enable rapid IC to the ground state. Computations for the open chain molecules resulted in barriers almost 1 eV above the energy minimum of the $^1n\pi^*$ state [9, 13], while smaller barriers of ~0.4 eV were obtained for the cyclic species studied in this work.

The dynamics becomes more complex upon excitation to the $^1\pi\pi^*$ state, as more reaction paths become accessible. Furthermore, the triplet yields vary considerably depending

on both the molecular structures and their environment. In acrolein and its methylated derivatives, the rate of IC between the $^1n\pi^*$ state and the singlet ground state was interpreted to depend on: (a) the large amplitude twisting motion of the terminal CH_2-group (a slower motion would follow from C3 methyl substitution), and (b) the 'velocity' of the wavepacket when passing through the region of a conical intersection, affecting diabatic vs. adiabatic branching (the critical coordinates [**g**- and **h**-vectors] were found to involve terminal twisting and pyramidalization at the C2-atom). The fastest relaxation to the ground state was observed for crotonaldehyde, which has a methyl group at the terminal C3-position, but not at the C2-position. The high quantum yield for IC to the ground state is only observed in the gas phase, where no internal energy is lost to the environment, and the barriers to conical intersections are readily surmounted. The rate of ISC, on the other hand, depends not only on the existence of large spin-orbit coupling, but also on the (near) degeneracy of singlet and triplet states [3, 7, 44] over an extended region of the potential energy surface in order to accumulate an appreciable transition amplitude. In that sense, the ISC rate for TMCPO is reduced, as indicated by calculations, due to a larger energy gap between the $^1n\pi^*$-minimum and the triplet states, most importantly for the preferred $^3\pi\pi^*$ state associated with El Sayed's rules.

In the present study, the role of large amplitude motions involving the carbon atoms which comprise the π-electron system was minimized by "locking down" the carbon backbone into a closed ring (with MVK as the exception which forms the basis for comparison). Examining the role of methylation in the absence of such large amplitude distortions, we find that both the triplet quantum yield and the triplet decay rate decrease upon methylation.

The emerging picture of dynamical processes following photoexcitation to the $^1\pi\pi^*$ state can be summarized as follows. The wavepacket immediately undergoes gradient-

directed relaxation and approaches the seam of conical intersection with the $^1n\pi^*$ state. As the wavepacket passes through this region, it may undergo nonadiabatic transition from the $^1\pi\pi^*$ to the $^1n\pi^*$ state, with the gradients on the latter surface directing the wavepacket toward the well-defined S_1 minimum or to the nearby S_0-S_1 conical intersections whereupon it reaches the ground state (i.e. internal conversion), as observed in other molecules having conjugated π-electron systems [26, 39, 45]. Alternatively, the initial wavepacket may continue diabatically through the S_2-S_1 coupling region, retaining $^1\pi\pi^*$ character for a longer period of time.

In the case of the current experiment, however, the predominant component of the wavepacket appears to develop $^1n\pi^*$-character. This is consistent with the analogous dynamical processes observed for acrolein. In the present case, one observes a higher triplet yield as well as a lower barrier to accessing the conical intersection to the ground state, suggesting that decay to the ground state via the $^1n\pi^*$ state is even more likely. Furthermore, it is assumed that all ISC processes initiate on the $^1n\pi^*$ state. A comparatively rapid decay rate (competitive with IC) requires relatively large spin-orbit coupling constants, as well as an energetically proximate triplet manifold over large regions of coordinate space. As discussed in Sec. IIIB and summarized in Tables 1 and 2, all the molecules in this study possess such features. Quantitatively, however, Table 3 shows the trend that increased methylation leads to a deceleration of ISC. Since the relevant computed spin-orbit coupling constants increase (slightly) with methylation, rationalizing this trend likely requires a dynamical perspective. Specifically, an identification of which coordinates and molecular vibrations are most closely associated with singlet-triplet state coupling is needed, as well as an understanding of the inertially retarding effects that methylation may have on these.

While the preceding analysis rationalizes the present results, it should be noted that the similar time scales for ISC and IC are largely dependent on the fact that the internal energy is conserved in gas phase processes. This is not the case in the liquid phase where energy dissipation rapidly decreases the internal vibrational energy to the extent that crossing to the ground state via conical intersections occurs at a much slower rate than ISC. This can be understood as solvent-induced relaxation rapidly bringing the system close to the S_1 minimum, energetically below the barriers which lead to S_0-S_1 intersection. This renders ISC the dominant solution phase relaxation pathway [23, 24].

These results suggest that cyclopentenone and its methylated derivatives form an "intermediate case" between the ultrafast gradient directed dynamics and processes which are better described by statistical theories. The photoinitiated dynamics of smaller polyenes are characterized by the former, displaying electronic relaxation on a sub-picosecond time scale, which in general is shorter than the timescales for intramolecular vibrational redistribution (IVR) [46, 47]. Non-adiabatic dynamical processes which occur on timescales shorter than those required for IVR limit the utility of "Golden Rule" based statistical descriptions, since not all degrees of freedom (e.g. low frequency modes) can be involved on such short time scales. That this intermediate regime is relevant in systems containing heteroatoms (particularly those characterized by large spin-orbit coupling) is a result of ISC occurring on a timescale competitive with the singlet relaxation processes. The present study on cyclic enones combined with the results of prior studies of linear enones [13] reveals that: the (gas phase) IC time scales in these systems range from 0.5 (crotonalhdehyde) to 3 ps (TMCPO); the ISC rate seems to be within the same order of magnitude whereas the quantum yields depend on the actual rates. In order to firmly establish these trends, however, experiments on still larger systems are desirable, as are more detailed ab initio dynamical investigations of these radiationless processes.

V. CONCLUSION

Time resolved photoelectron spectroscopy was employed to investigate the excited state dynamics, following excitation to their lowest lying $^1\pi\pi^*$ state, of the cyclic α,β-enones cyclopentenone and its methylated derivatives, cyclohexenone and the open chain methyl vinyl ketone. Following rapid electronic relaxation on a 100 fs timescale, the system either returns to the ground state or undergo ISC via the $^1n\pi^*$ state. The triplet yields vary between 0.35 and 0.08 and show that, for the molecules studied here, both channels are accessed . Increased methylation decelerates both ISC and IC, as detailed in the discussion section. That ISC can compete with IC depends on two factors, which seem to be a pattern in the photodynamics of α, β unsaturated carbonyls: (i) there is a significant barrier to accessing the conical intersection between the $^1n\pi^*$ state and the ground state from the $^1n\pi^*$-minimum energy geometry (in contrast to simple polyenes where this crossing is close to the energetic minimum); and (ii) energetically close lying $^3\pi\pi^*$-triplet states exist over large regions of configuration space, leading to high ISC probabilities and, therefore, quick access to the triplet manifold.

In a future study, we plan to investigate these dynamics in liquid phase enones, where (i) the solvent polarity can influence the energies of conical intersections and triplet states and (ii) vibrational energy can be dissipated into the surrounding solvent.

Associated content

Supporting Information

Detailed analysis of the $^1\pi\pi^*$ band in the photoelectron spectra for 3MeCPO and TMCPO; He(I) photoelectron spectra of CPO, 3MeCPO and TMCPO and time resolved photoelectron

spectra of MVK; details on the decay and SAS (Section IV.1 and Figure 6); geometries of minima and conical intersections discussed in the manuscript. This content is available free of charge via the internet at http://pubs.asc.org.

Author Information

Corresponding Author

* Electronic address: albert.stolow@nrc-cnrc.gc.ca

Notes

The authors declare no competing financial interest.

Acknowledgements

This work was supported by NSERC Canada, the DFG-Cluster of Excellence: Munich Center of Advanced Photonics, Germany; the Swedish Research Council (VR), the Knut and Alice Wallenberg Foundation, and the Göran Gustafsson Foundation, Sweden. O.S. gratefully acknowledges financial support from the Humboldt Society, Germany, and the Wenner-Gren Foundation, Sweden. We thank Prof. E. Riedle for stimulating discussions and support of this effort.

References

[1] Richard, R.; Sauvage, P.; Wan, C. S. K.; Weedon, A. C.; Wong, D. F. Photochemical Enolization of Acyclic β-alkyl-α,β-unsaturated Ketones. *J. Org Chem.* **1986**, *51*, 62-67.

[2] Wolff, S.; Schreiber, W. L.; Smith II, A. B.; Agosta, W. C. Photochemistry of Cyclopentenones. Hydrogen Abstraction by the β-Carbon Atom. *J. Am. Chem. Soc.* **1972**, *94*, 7797-7806.

[3] Su, M.-D. The Role of Spin-Orbit Coupling and Symmetry in Photochemical Rearrangements of α,β-Unsaturated Cyclic Ketones. *Chem. Phys.* **1996**, *205*, 277-308.

[4] Carey, F. A.; Sundberg, R. J. *Organische Chemie*, volume 1. Wiley VCH, Weinheim, 1995.

[5] Fang, W.-H. A CASSCF Study on Photodissociation of Acrolein in the Gas Phase. *J. Am. Chem. Soc.* **1999,** *121*, 8376-8384.

[6] Aquilante, F.; Barone, V.; Roos. O. B. A Theoretical Investigation of Valence and Rydberg Electronic States of Acrolein. *J. Chem. Phys.* **2003**, *119*, 12323-12334.

[7] Beljonne, D.; Shuai, Z.; Pourtois, G.; Bredas, J. L. Spin-Orbit Coupling and Intersystem Crossing in Conjugated Polymers: A Configuration Interaction Description. *J. Phys. Chem. A* **2001,** *105,* 3899-3907.

[8] El-Sayed, M. A. Spin-Orbit Coupling and the Radiationless Processes in Nitrogen Heterocyclics. *J. Chem. Phys.* **1963**, *38*, 2834-2838.

[9] Reguero, M.; Olivucci, M.; Bernardi, F.; Robb, M. A. Excited-State Potential Surface Crossings in Acrolein: A Model for Understanding the Photochemistry and Photophysics of α,β-Enones. *J. Am Chem. Soc.* **1994**, *116*, 2103-2114.

[10] Garcia-Exposito, E.; Bearpark, M. J.; Ortuno, R. M.; Branchdell, V.; Robb, M. A.;

Wilsey, S. J. Org. Chem. The T_1 $^3(\pi-\pi^*)/S_0$ Intersections and Triplet Lifetimes of Cyclic α,β-Enones. *J. Org. Chem.* **2001**, *66*, 8811-8814.

[11] Wu, W.; Yang, C.; Zhao, H.; Liu, K.; Su, H. Photodissociation and Photoisomerization Dynamics of CH2=CHCHO in Solution. *J. Chem. Phys.*, **2010**, *132* 124510 1-10.

[12] Parsons, B. F.; Szpunar, D. E.; Buttler, L. J. H-Atom High-n Rydberg Time-of-Flight Spectroscopy of C–H Bond Fission in Acrolein Dissociated at 193 nm. *J. Chem. Phys.* **2002**, *117*, 7889-7895.

[13] Lee, A. M. D.; Coe, J. D.; Ullrich, S.; Ho, M.-L.; Lee, S.-J.; Cheng,B.-M.; Zgierski, M. Z.; Chen, I.-C.; Martinez, T. J.; Stolow, A. Substituent Effects on Dynamics at Conical Intersections: α,β-Enones. *J. Phys. Chem. A*, **2007**, *111*, 11948-11960.

[14] Haas, B. M.; Minton, T. K.; Felder, P.; Huber, J. R. Photodissociation of Acrolein and Propynal at 193 nm in a Molecular Beam. Primary and Secondary Reactions. *J. Phys. Chem.* **1991**, *95*, 5149-5159.

[15] Shu, J.; Peterka, D. S.; Leone, S. R.; Ahmed. M. J. Tunable Synchrotron Vacuum Ultraviolet Ionization, Time-of-Flight Investigation of the Photodissociation of trans-Crotonaldehyde at 193 nm. *Phys. Chem. A* **2004**, *108*, 7895-7902.

[16] Kao, Y.-T.; Chen, W.-C.; Yu, C.-H.; Chen, I.-C. Production of HCO from Propenal Photolyzed at 193 nm: Relaxation of Excited States and Distribution of Internal States of Fragment HCO. *J. Chem. Phys.* **2001**, *114*, 8964-8970.

[17] Paulisse, K. W.; Friday, T. O.; Graske, M. L.; Polik. M. F. Vibronic Spectroscopy and Lifetime of S_1 Acrolein. *J. Chem. Phys.* **2000***, 113*, 184-191.

[18] Reguero, M.; Bernardi, F.; Olivucci, M.; Robb, M. A. A Model Study of the Mechanism of the Type B (Di-π-methane) and Lumiketone Rearrangement in Rotationally

Constrained α,β-Enones. *J. Org. Chem.* **1997**, *62*, 6897-6902.

[19] Bonneau, R. Transient Species in Photochemistry of Enones. The Orthogonal Triplet State Revealed by Laser Photolysis. *J. Am. Chem. Soc.* **1980**, *102*, 3816-3822.

[20] Caldwell, R. A.; Tang, W.; Heibel, G. E.; Schuster, D. I. Nanosecond Kinetic Absorption and Calorimetric studies of Cyclopentenone: The Triplet, self-quenching, and the Predimerization Biradicals. *Photochem. Photobiol.*, **1991**, *53*, 159.

[21] Schuster D. I.; Dunn, D.A.; Heibel, G. E.; Brown, P. B.; Rao, J. M.; Woning J.; Bonneau, R. Dynamic Properties of Triplet Excited States of Cyclic Conjugated Enones as Revealed by Transient Absorption Spectroscopy. *J. Am. Chem. Soc.* **1991**, *113*, 6245-6255.

[22] Devaquet, A. Potential Energy Sheets for the nπ* and ππ* Triplet States of α,β-Unsaturated Ketones. *J. Am. Chem. Soc*. **1972,** *94*, 5160-5167.

[23] Schalk, O.; Lang, P.; Wu, G.; Schuurman, M. S.; Riedle, E.; Stolow, A.; Internal Conversion vs. Intersystem Crossing – What Drives the Dynamics of Cyclic α,β-Enones? Ultrafast Phenomena XVIII, EPJ Web of Conferences 41, 02031 (2013).

[24] Riedle, E.; Bradler, M.; Sailer, C.; Wenninger, M.; Pugliesi, I. Electronic Transient Spectroscopy from the Deep UV to the NIR: Unambiguous Disentanglement of Complex Processes. *Faraday Discussion* **2013**, *163*, 139-158.

[25] Wu, G.; Boguslavskiy, A. E.; Schalk, O.; Schuurman, M. S.; Stolow, A. Ultrafast Non-adaibatic Dynamics of Methyl Substituted Ethylenes. *J. Chem. Phys.* **2011**, *135*, 164309.

[26] Schalk, O.; Boguslavskiy, A. E.; Stolow, A.; Schuurman, M., Through-Bond Interactions and the Localization of Excited-State Dynamics. *J. Am. Chem. Soc.* **2011**, *133*, 16451-

16458.

[27] Eland, J. H. D.; Vieuxmaire, O.; Kinugawa, T.; Lablanquie, P.; Hall, R. I.; Penent, F. Complete Two-Electron Spectra in Double Photoionization: The Rare Gases Ar, Kr, and Xe. *Phys. Rev. Lett.* **2003**, *90*, 053003.

[28] Eland, J. H. D.; Feifel, R. Double Ionization of ICN and BrCN Studied by a New Photoelectron-Photoion Coincidence Technique. *Chem. Phys.* **2006**, *327*, 85-90.

[29] Feifel, R.; Eland, J. H. D.; Storchi, L.; Tarantelli F. An Experimental and Theoretical Study of Double Photoionization of CF4 Using Time-of-Flight Photoelectron-Photoelectron (Photoion-Photoion) Coincidence Spectroscopy. *J. Chem. Phys.* **2006**, *125*, 194318.

[30] Lochbrunner, S.; Larsen, J.; Shaffer, J.; Schmitt, M.; Schultz, T.; Underwood, J.; Stolow, A., Methods and Applications of Femtosecond Time-Resolved Photoelectron Spectroscopy. *J. Electron Spectrosc. Relat. Phenom.* **2000,** *112*, 183-198.

[31] Even, U,; Jortner, J.; Noy, D.; Lavie, N.; Cossart-Magos, C. Cooling of Large Molecules Below 1 K and He Clusters Formation. *J. Chem. Phys.* **2000**, *112*, 8068–8071.

[32] Pierloot, K.; Dumez, B.; Widmar P.-O.; Roos, B. O. Density-Matrix Averaged Atomic Natural Orbital (ANO) Basis-Sets for Correlated Molecular Wave-Functions. 4. Medium-Sized Basis-Sets for the Atoms H-Kr. *Theor. Chem. Acc.* **1995**, *90*, 87-114.

[33] Stanton, J. F.; Gauss, J.; Harding, M. E.; Szalay, P. G. 32, Coupled-Cluster techniques for Computational Chemistry, a quantum-chemical program package. Current version: http://www.32.de.

[34] Lischka, H.; Shepard, R.; Shavitt, I.; Pitzer, R. M.; Dallos, M.; Müller, Th. ; Szalay, P. G.; Brown, F. B.; Ahlrichs, R.; Böhm, H. J. et. al. COLUMBUS, an Ab Initio Electronic Structure Program, Release 7.0 (2012).

[35] Langhoff, S. R.; Davidson, E. R. Configuration Interaction Calculations on the Nitrogen Molecule. *Int. J. Quant. Chem.* **1974**, *8*, 61–72.

[36] Werner, H.-J.; Knowles, P. J.; Knizia, G.; Manby, F. R.; Schütz, M.; Celani, P.; Koronea, T.; Lidh, R.; Mitrushenkov, A.; Rauhut, G. et al. MOLPRO, Version 2012.1, A Package of Ab Initio Programs, Cardiff, UK, 2012. Current Version: http://www.molpro.net.

[37] Masclet, P.; Mouvier, G. Étude par Spectrométrie Photoelectronique d'Aldéhydes et de Cétones Éthélyniques Conjugés. *J. Electron. Spectrosc. Relat. Phenom.* **1978**, *14,* 77-97.

[38] Kimura, K.; Katsumata, S.; Achiba, Y.; Yamazaki, Y.; Iwata, S. *Handbook of HeI Photoelectron Spectra of Fundamental Organic Molecules*. Japan Scientific Societies Press, Tokyo, 1981.

[39] Levine, B. G.; Martinez, T. J. Isomerization Through Conical Intersections. *Annu. Rev. Phys. Chem.* **2007,** *58,* 613-634.

[40] Stolow, A.; Underwood, J. G. Time-Resolved Photoelectron Spectroscopy of Nonadiabatic Dynamics in Polyatomic Molecules. *Adv. Chem. Phys.*, **2008**, *139*, 497-583.

[41] Schalk, O.; Boguslavskiy, A. E.; Stolow, A., Substituent Effects on Dynamics at Conical Intersections: Cyclopentadienes. *J. Phys. Chem. A* **2010,** *114*, 4058-4064.

[42] Schalk, O.; Boguslavskiy, A. E.; Schuurman, M. S.; Broogard, R. Y.; Unterreiner, A. N.; Wrona-Piotrowicz, A.; Werstiuk, N. H.; Stolow, A. Substituent Effects on Dynamics at Conical Intersections: Cycloheptatrienes. *J. Phys Chem A* **2013,** *117,* 10239-10247.

[43] Cheatham, C. M.; Laane, J The Jet-Cooled Fluorescence Excitation Spectrum and Ring-Bending Potential Energy Function and Conformation of 2-Cyclopenten-l-one in the S_1

(nπ*) Electronic Excited State. *J. Chem. Phys.* **1991**, *94*, 7734-7743.

[44] McGlynn, S. P.; Azumi, T.; Kinoshita, M. *Molecular Spectroscopy of the Triplet State*, Prentice Hall, New York, 1969.

[45] Kuhlman, T. S.; Glover, W. J.; Mori, T.; Moller, K. B.; Martinez, T. J. Between Ethylene and Polyenes - the Non-Adiabatic Dynamics of cis-Dienes. *Faraday Disussions* **2012,** *157,* 193-212.

[46] Nesbitt, D. J.; Field, R. W. Vibrational Energy Flow in Highly Excited Molecules: Role of Intramolecular Vibrational Redistribution. *J. Phys. Chem.* **1996**, *100,* 12735-12756.

[47] Schalk, O.; Unterreiner, A.-U. Vibrational Cooling in the Liquid Phase Studied by Ultrafast Investigations of Cycloheptatriene. *Mol. Phys.* **2009**, *107*, 2159-2167.

Figures

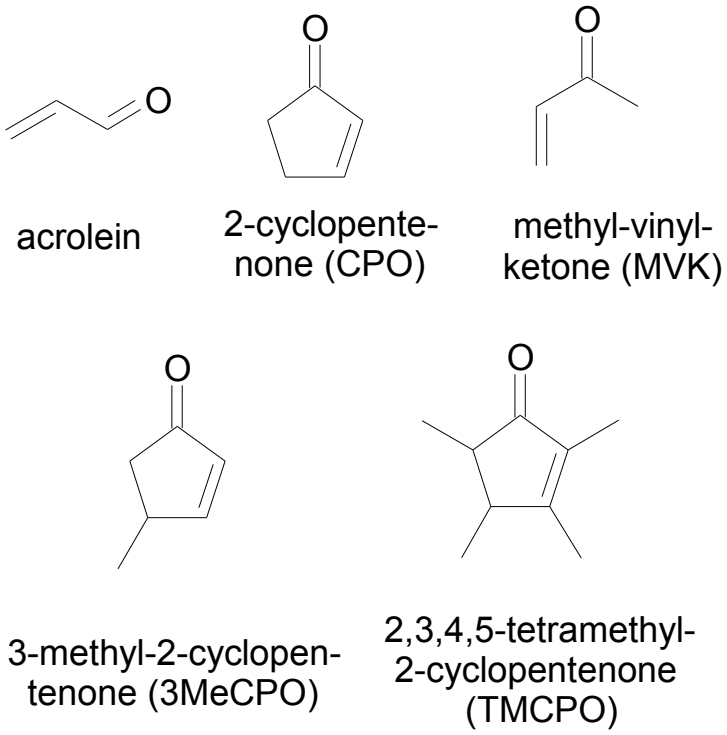

Figure 1. Structures of the molecules under study.

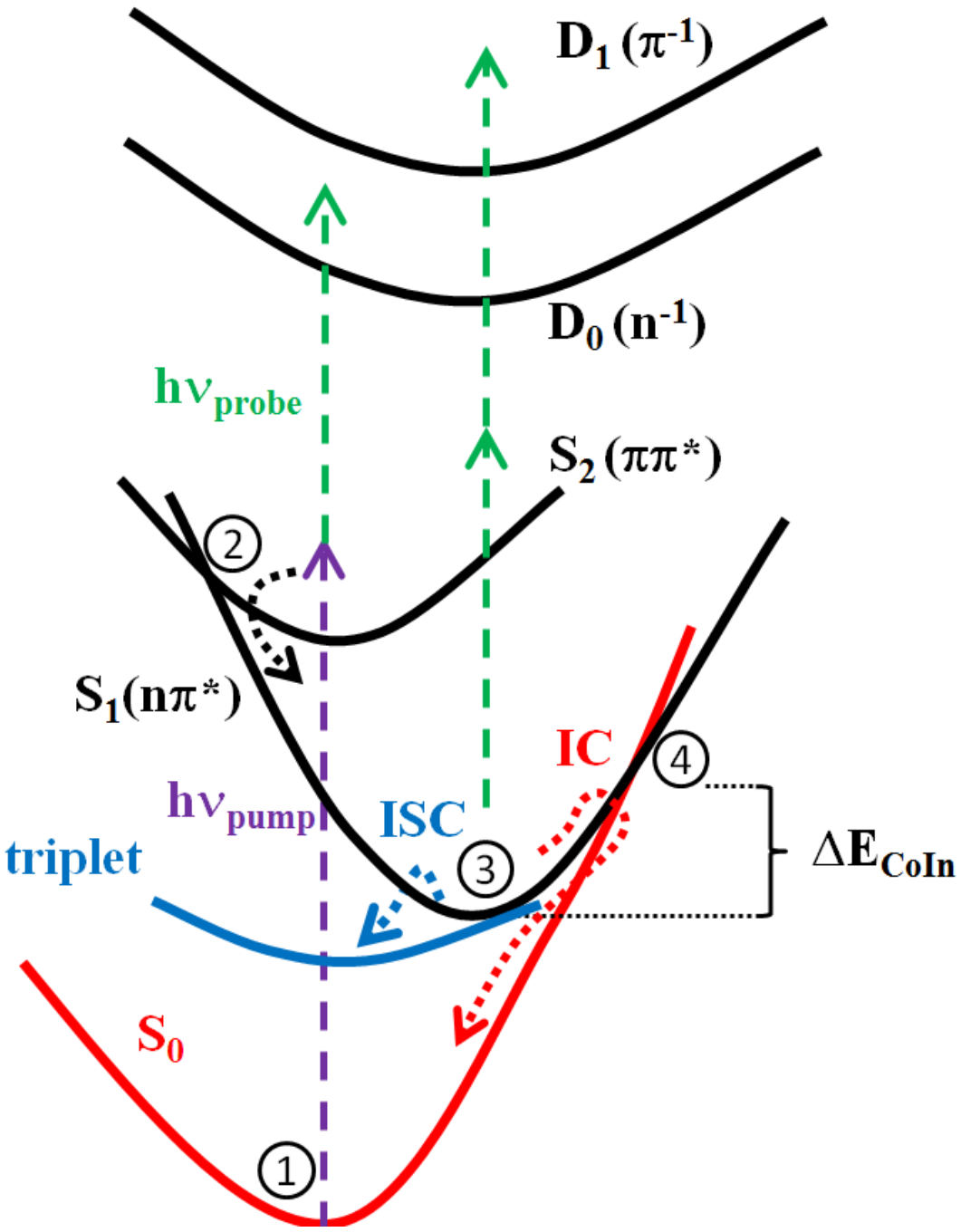

Figure 2. Sketch of the photo-induced dynamics of acrolein, 2-cyclopentenone (CPO) and its methylated derivatives upon excitation to the $S_2(\pi\pi^*)$ state as detailed in the text. Geometries for CPO at the positions indicated by the numbers are shown in Figure 5.

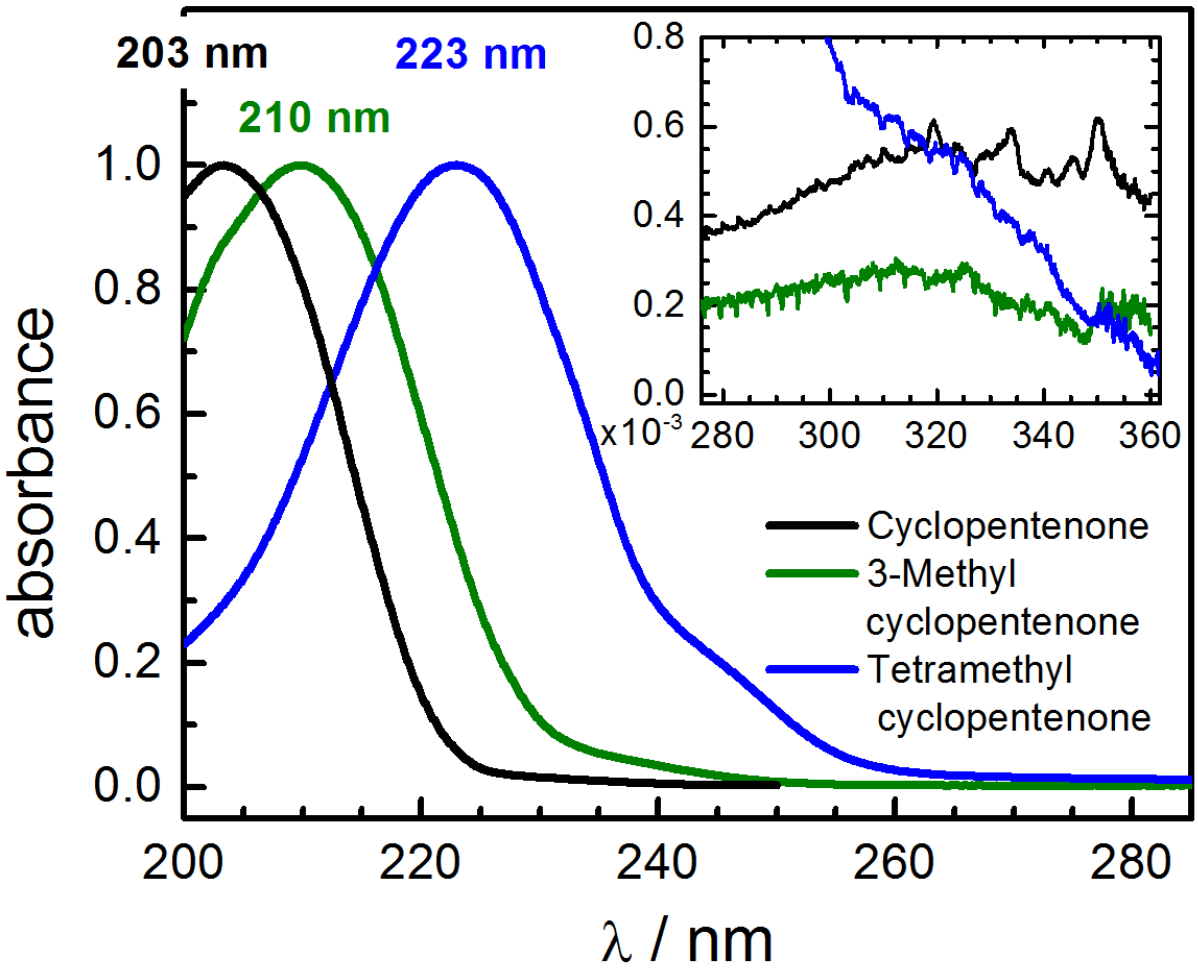

Figure 3. Gas phase absorption spectra of 2-cyclopentenone (black), 3-methyl-2-cyclopentenone (green) and 2,3,4,5-tetramethyl-2-cyclopentenone (blue).

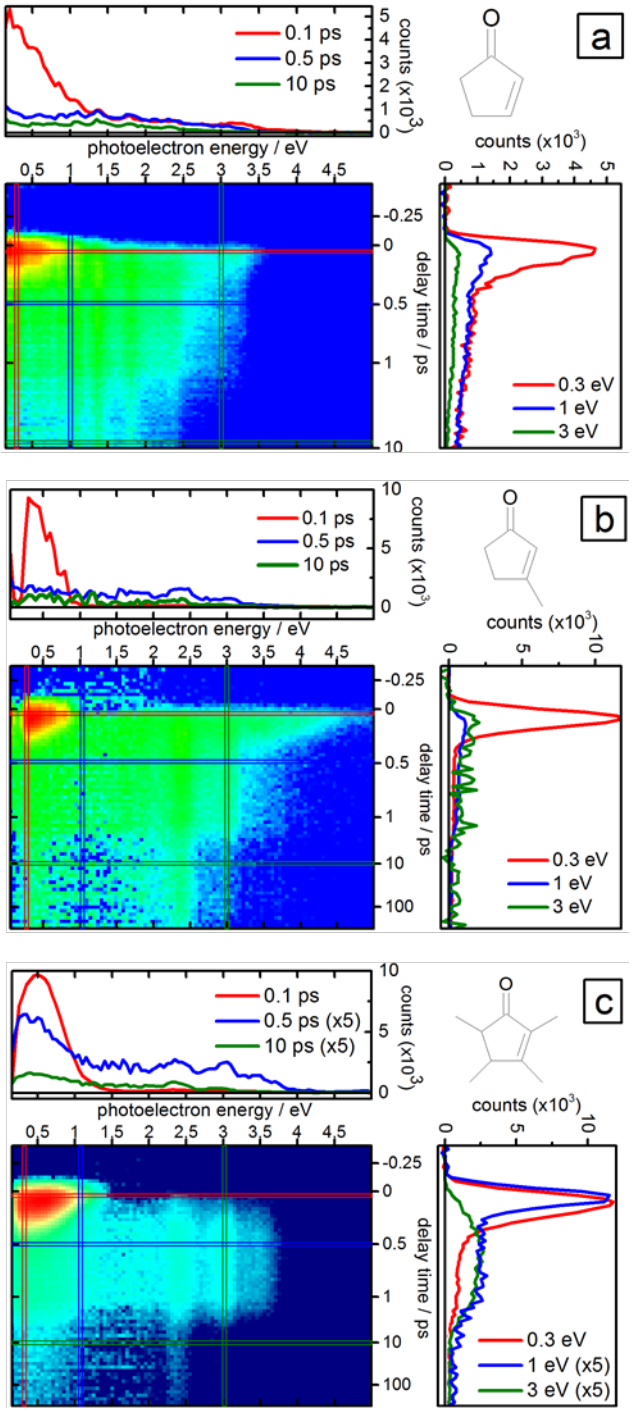

Figure 4. Time-resolved photoelectron (TRPES) spectra of a) 2-cyclopentenone, b) 3-methyl-2-cyclopentenone and c) 2,3,4,5-tetramethyl-2-cyclopentenone after excitation at 216 nm and probing at 267 nm. Time slices at delays of 0.1, 0.5 and 10 ps are shown above each TRPES spectrum; energy slices at 0.3, 1, and 3 eV are shown on the right hand side of each TRPES spectrum.

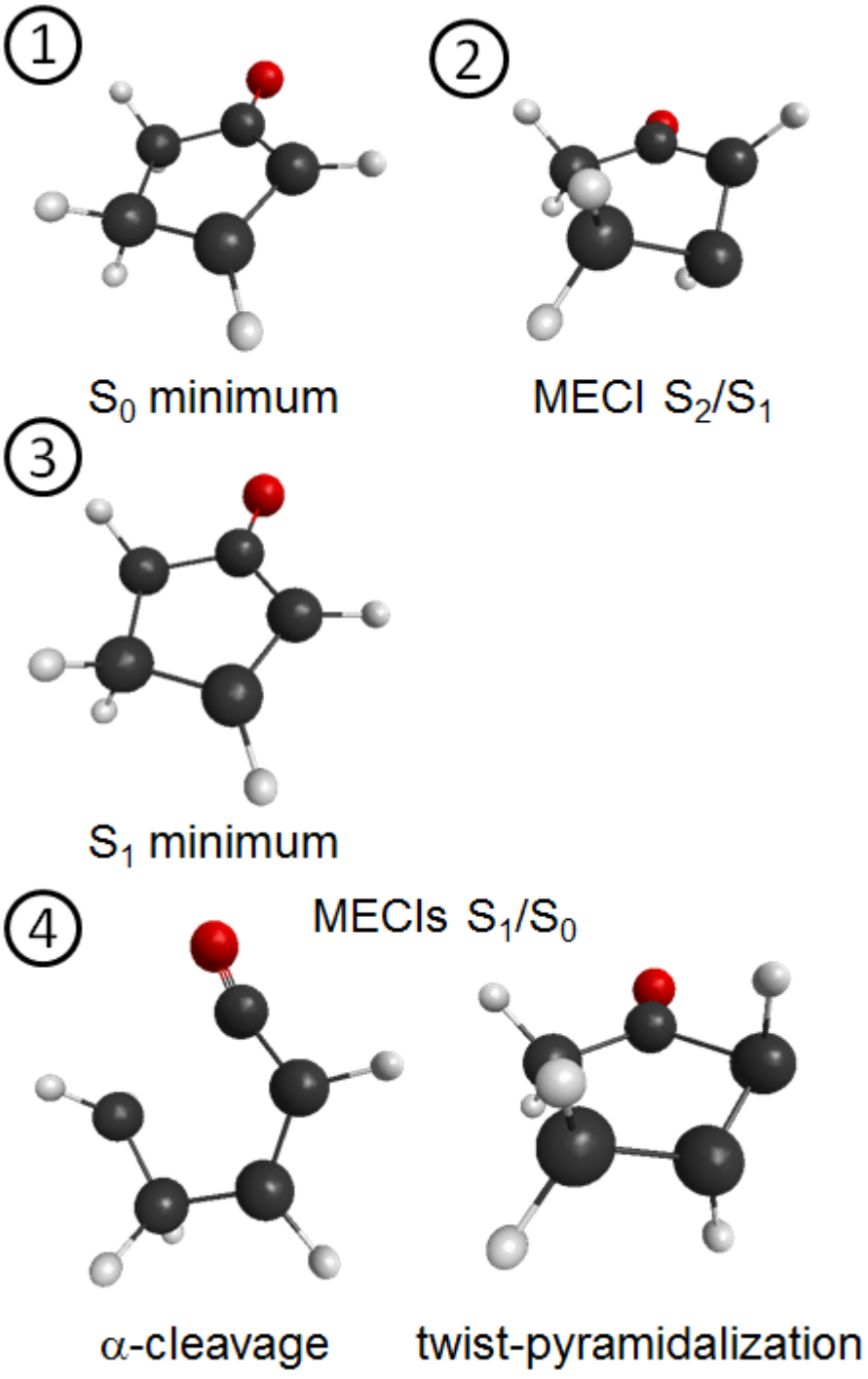

Figure 5. Relevant geometries in the reaction path according to the numbering in Figure 4: The lowest lying MECIs between the $^1n\pi^*$ (S_1) state and the ground state is the ring-opened α-cleavage form which lies below the *ortho* twisted-pyramidalized form.

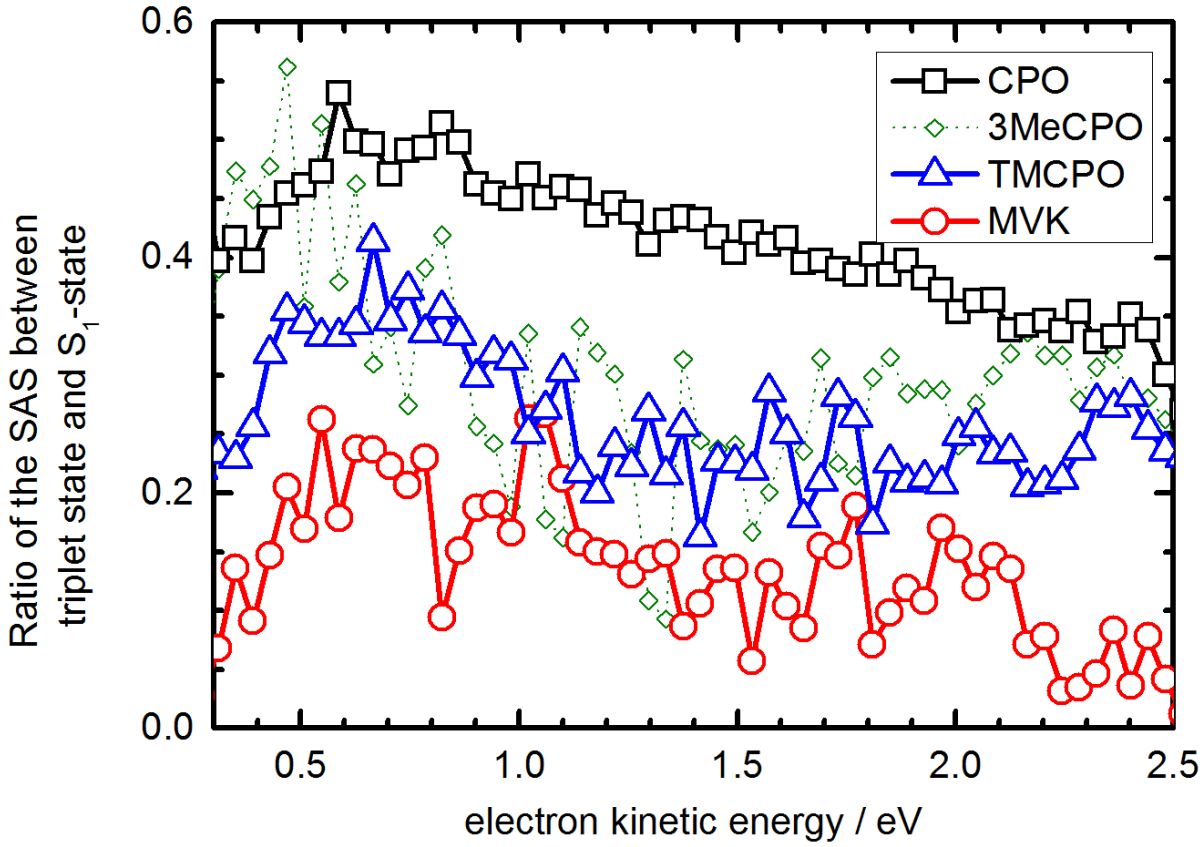

Figure 6. Ratio between state associated spectra (SAS) of the long-time component of the triplet state signal and the $^1n\pi^*$-decay time $A(\tau_2)$ for: 2-cyclopentenone (CPO, black squares), 3-methyl-2-cyclopentenone (3MeCPO, small green tilted squares), 2,3,4,5-tetramethyl-2-cyclopentenone (TMCPO, blue triangles), and methyl-vinyl-ketone (MVK, red circles).

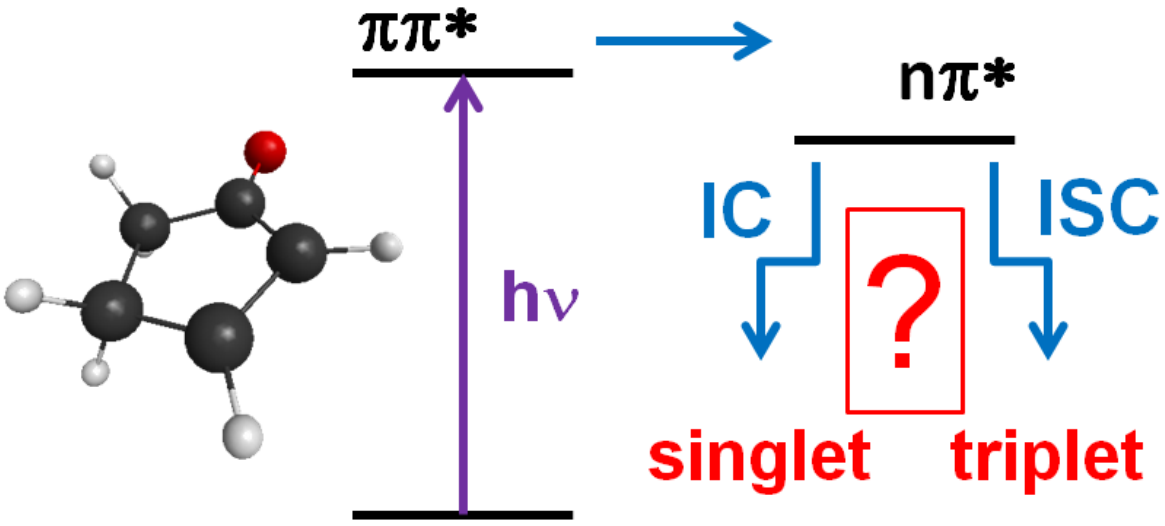

Figure for Table of Contents.

Tables

Table 1. Ground and excited state energies (in eV) at adiabatic surface minima for CPO, 3MeCPO, and TMCPO.[a]

	CPO		3MeCPO		TMCPO	
	R_{min} (S_0)	R_{min} (S_1)	R_{min} (S_0)	R_{min} (S_1)	R_{min} (S_0)	R_{min} (S_1)
S_0, A’	0.00	0.65	0.00	0.52	0.00	0.59
$S_1(n\pi^*)$, A”	4.01	3.56	4.05	3.63	4.18	3.77
$S_2(\pi\pi^*)$, A’	6.17	6.26	6.11	6.36	5.84	5.56
$S_3(n\pi^*)$, A”	6.93	6.51	6.95	6.60	6.87	6.82
$T_1(n\pi^*)$, A”	3.83	3.42	3.85	3.49	3.69	3.25
$T_2(\pi\pi^*)$, A’	4.04	3.70	4.07	3.74	3.98	3.53
$T_3(\pi\pi^*)$, A’	6.27	5.88	6.26	5.96	6.48	6.02
$T_4(n\pi^*)$, A”	6.84	6.74	6.86	6.74	6.71	6.68

[a] Computed at the Davidson corrected SO-MRCI/CASSCF(6,5) level of theory. C_S symmetry is indicated by labels of the irreducible representation, although TMCPO doses not posess C_s symmetry.

Table 2. Ground and excited state energies (in eV) at minimum energy conical intersections of CPO, 3MeCPO, and TMCPO.[a]

	CPO				3MeCPO				TMCPO			
	R_{mex} (S_2-S_1)		R_{mex} (S_1-S_0)		R_{mex} (S_2-S_1)		R_{mex} (S_1-S_0)		R_{mex} (S_2-S_1)		R_{mex} (S_1-S_0)	
	α-cleave	twist/pyr..	α-cleave	twist/pyr.	α-cleave	twist/pyr.	α-cleave	twist/pyr.	α-cleave	twist/pyr.	α-cleave	twist/pyr.
S_0	4.76	4.29	3.93	4.78	4.99	4.25	3.95	4.43	5.13	3.91	4.10	4.81
S_1	5.63	5.55	3.93	4.78	5.71	5.43	3.95	4.43	6.00	5.41	4.10	4.81
S_2	5.63	5.55	7.56	8.15	5.71	5.43	7.51	7.36	6.00	5.41	8.08	7.28
S_3	9.40	9.10	9.40	8.54	9.81	9.07	9.11	9.38	9.91	8.82	8.40	9.58
T_1	5.25	4.90	3.88	5.13	5.01	4.75	4.17	4.59	5.27	4.51	4.33	4.99
T_2	6.23	6.02	7.21	7.26	5.75	5.85	5.78	6.87	6.01	5.79	6.06	7.06
T_3	8.33	9.00	7.84	8.17	9.71	8.94	7.20	8.00	9.72	8.71	7.13	8.46
T_4	9.35	9.86	9.15	9.84	9.86	9.45	9.21	9.31	9.89	9.57	9.34	9.54

[a] All energies are relative to the ground state minimum energy of the respective molecule at the SO-MRCI/CASSCF(6,5) level of theory.

Table 3. Time constants τ_1 and τ_2 obtained by a global fitting analysis from the time-resolved photoelectron spectra, estimated triplet quantum yields Φ_{ISC} and time constants for internal conversion τ_{IC} and intersystem crossing τ_{ISC}. See text and supporting information for details.

	τ_1 / fs	τ_2 / ps	Φ_{ISC}	τ_{IC} / ps	τ_{ISC} / ps
CPO	120	1.2	0.35	1.8	3.5
3MeCPO	90	1.4	0.23	1.8	6.1
TMCPO	160	2.8	0.21	3.5	13
MVK	50	0.9	0.12	1.0	7.5